Physical mechanisms of thermal-diffusivity depth-profile generation in a hardened low-alloy Mn, Si, Cr, Mo steel reconstructed by photothermal radiometry

Lena Nicolaides and Andreas Mandelis[a)]
Photothermal and Optoelectronic Diagnostics Laboratories, Department of Mechanical and Industrial Engineering, University of Toronto, 5 King's College Road, Toronto, Ontario, Canada M5S 3G8

Clare J. Beingessner
B & W Heat Treating Ltd., 390 Trillium Drive, Kitchener, Ontario, Canada N2G 4W6

(Received 26 September 2000; accepted for publication 29 March 2001)

It is well established that in hardened steels thermal-diffusivity broadly anticorrelates with microhardness, allowing thermal-wave depth profilometry to be used as a tool to measure microhardness profiles. Nevertheless, the physical mechanisms for this anticorrelation have not been well understood. In this work, the thermal-diffusivity profiles of rough, hardened industrial steels were reconstructed after the elimination of roughness effects from the experimental data. Carburizing and quenching are widely used for the heat treatment of steel components, and it is important to understand their effects on thermal-diffusivity profiles. A thorough examination of the actual mechanism by which thermal-diffusivity depth profiles are affected by first carburizing and then quenching AISI-8620 steels was performed. It was concluded that the variation of thermal diffusivity with depth is dominated by the carbon concentration profile, whereas the *absolute value* of the thermal diffusivity is a function of microstructure. © *2001 American Institute of Physics.* [DOI: 10.1063/1.1373698]

I. INTRODUCTION

Depth profilometry is an important thermal-wave inverse problem where the thermal-diffusivity profile is reconstructed from the experimental surface information. Thermal diffusivity is the transport property that depends on the microstructural properties of a material, among other properties, and can thus be used to identify changes that take place as a result of surface or bulk modification processes, such as laser processing, case hardening, and coating deposition.[1] For determining the metallurgical properties of case-treated materials, depth profilometry offers an important advantage over existing techniques by being a nondestructive method. Since microhardness testing is a time-consuming and costly process, there is a demand for nondestructive testing in the heat-treating industry. A photothermal nondestructive method which can monitor hardness (indirectly), would be an important achievement. From the point of view of quantitative depth profilometry, just as important is the elucidation of the physical mechanism(s) that give rise to the thermophysical (thermal-diffusivity) depth profile in a given steel. With inhomogeneous materials, the photothermal amplitude and phase signal channels carry information about any heat-transport disruption or change below the surface. These changes must be interpreted with appropriate thermal-wave models, in order to yield reliable reconstructions of the spatially variant thermal diffusivity of a sample.

To understand the mechanism by which the thermal-diffusivity profile in carburized and hardened steels develops, AISI-8620 steel samples were chosen for testing. Its chemical composition contains 0.18/0.23% C, 0.70/0.90% Mn, 0.40/0.70 Ni, 0.40/0.60% Cr and 0.15/0.25% Mo. AISI-8620 is a popular low-carbon, low-alloy steel owing to its ability to produce high-core strength and toughness and is widely used in such applications as gears, pinions, small engine crankshafts, etc. In earlier studies,[2,3] inverse thermal-wave problem types of reconstructions were performed on quenched steels, and anticorrelation trends between thermal diffusivity and hardness were found. However, no physical interpretation of the depth profiles was given other than the evidence that the microstructure anticorrelates with thermal diffusivity. In this work, a set of samples was first studied after carburizing and then after quenching. The two processes, which are usually performed sequentially to produce a quenched steel, were studied in independent steps so that the origins of the thermal-diffusivity profiles would be understood in detail. Furthermore, in a laboratory study, neglecting surface roughness does not appear to be a severe limitation because rough samples can be easily polished. However, as an on-line industrial application, this technique would be prohibitively time consuming. Therefore, it is of great interest to incorporate the effects of roughness on the forward experimental data. With these goals in mind, a sample matrix was constructed as a function of roughness and case depth.

II. EXPERIMENTAL SETUP

In order to avoid unnecessary theoretical signal dimensionality complications,[4] thermal-wave depth profilometry is usually performed in the one-dimensional (depth-only) limit.

a)Electronic mail: mandelis@mie.utoronto.ca

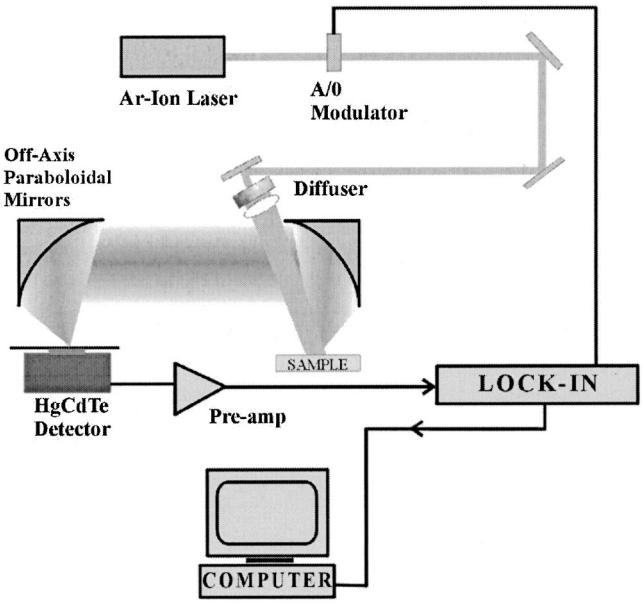

FIG. 1. Frequency-domain photothermal radiometric instrumentation for thermal-diffusivity depth profilometry.

Therefore, the experimental setup has a low spatial resolution. To maintain the one-dimensional heat diffusion formalism assumed in the theory, the pump laser beam spot size must be made much larger than the maximum profile depth and its intensity spatial profile must be flat. The experimental apparatus is shown in Fig. 1. A 514.5-nm-wavelength continuous-wave (cw) Innova Ar^+ laser from Coherent is modulated and then focused onto a sample at an output power of 1 W. To achieve a broad beam size (10 mm diam), an optical diffuser (5-mm-thick polymeric substrate) is placed in the path of the beam and the transmitted scattered light is collimated with a lens onto the surface of the sample. The modulation is performed by an external acousto-optic modulator (ISOMET 1201E-1). The blackbody radiation from the optically excited sample is collected and collimated by two silver-coated, off-axis paraboloidal mirrors and then focused onto a liquid-nitrogen-cooled HgCdTe (mercury–cadmium–telluride) detector (EG&G Judson model J15D12-M204-S01M). The heated area of the sample is at the focal point of the one mirror positioned near the sample, and the detector is at the focal point of the other mirror. The HgCdTe detector is a photoconductive element that undergoes a change in resistance proportional to the intensity of the incident infrared radiation. It has an active square size of 1 mm $\times$ 1 mm and a bandwidth of 2–12 μm. Since the efficiency of the detector increases with decreasing temperature, the detector is operated at a cryogenic temperature of 77 K. An antireflection-coated germanium window with a transmission bandwidth of 2–14 μm is mounted in front of the detector to block any visible synchronous radiation from the pump laser. Prior to being sent to the digital lock-in amplifier (Stanford Research Systems model SR850), the photothermal radiometric signal is amplified by a preamplifier (Analog Modules 350-3A), especially designed for operation with the HgCdTe detector. The low-noise preamplifier ensures a proper performance for subsequent signal processing with a lock-in amplifier. This process of data acquisition, storage, and scanning is fully automated.

TABLE I. AISI-8620 steel sample matrix arranged by roughness level and case depth.

Case depth	**0.02** in. (0.5 mm)	**0.04** in. (1.0 mm)	**0.06** in. (1.5 mm)
200 grit	Sample **11**	Sample **14**	Sample **17**
	Sample **12**	Sample **15**	Sample **18**
(~5 μm)	Sample **13**	Sample **16**	Sample **19**
600 grit	Sample **21**	Sample **24**	Sample **27**
	Sample **22**	Sample **25**	Sample **28**
(~2.5 μm)	Sample **23**	Sample **26**	Sample **29**
Hardness test samples	Sample **34**	Sample **35**	Sample **36**

III. HARDENED STEELS

Experimentally, a sample matrix was constructed as a function of roughness and case depth. AISI-8620 steel samples were first carburized to nominal case depths of 0.508 mm (0.02 in.), 1.016 mm (0.04 in.), and 1.524 mm (0.06 in.) and then quenched. The sample matrix is shown in Table I, and for each possible case three samples were studied for statistical purposes. Also, three samples (34, 35, and 36), representing each case-depth category, were used for microhardness testing. The samples used were 1 cm thick, and were cut from the same slab of AISI-8620 steel alloy. The surface roughness of the samples was controlled, before carburizing or quenching, with a 200 grit silicon carbide (SiC) grinding paper for samples 11–19, and with a 600 grit SiC grinding paper for samples 21–29. The average roughness d of each sample was measured independently with a surfometer (Series 400; Precision Devices, Milan, MI) of a 0.01 μm total system resolution. The instrument measures over an evaluation length, which is the length over which the surface parameters are evaluated. The evaluation length (10 mm) for each measurement consisted of five sampling lengths, where the sampling length is defined as the nominal wavelength used for separating roughness and waviness. For each measurement, the following three surface parameters were documented: (1) roughness average R_a, (2) maximum height of the profile R_t, and (3) average maximum height of the profile R_z. R_a is the arithmetic average of the absolute values of the profile heights over the evaluation length, R_t is the vertical distance between the highest and lowest points of the profile within the evaluation length, and R_z is the average of the successive values of R_{ti} (R_t of each sampling length) calculated over the evaluation length. The measurements were repeated at three independent positions on the surface of the sample, and the final value of each surface parameter was obtained as an average of the three measurements. For theoretical fitting the average of three independent R_z values, $\mathrm{avg}_3(R_z)$, was used as the roughness thickness d. This parameter was chosen as the effective thickness that generates

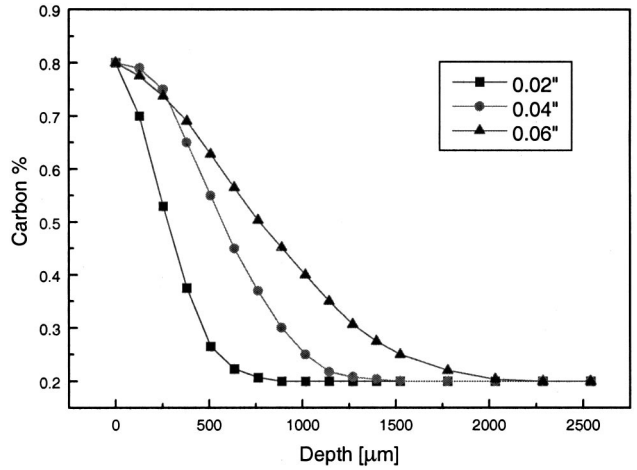

FIG. 2. Predicted (not measured) carbon profiles for case depths 0.02 in. (0.5 mm), 0.04 in. (1 mm), and 0.06 in. (1.5 mm) in AISI-8620 steel.

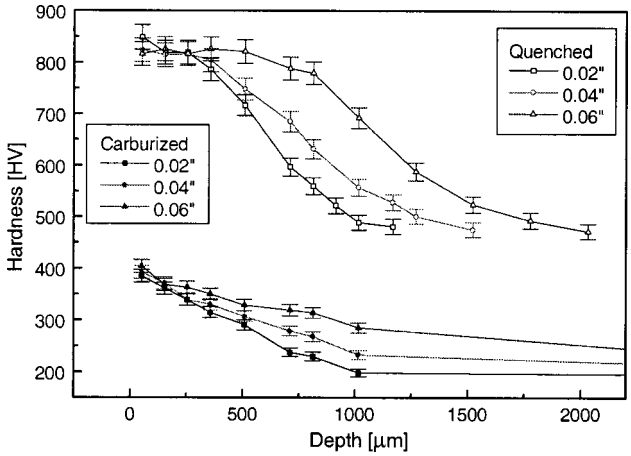

FIG. 3. Hardness profiles for carburized and quenched AISI-8620 samples of case depths 0.02 in. (0.5 mm), 0.04 in. (1.0 mm), and 0.06 in. (1.5 mm).

the photothermal signal that can be modeled as a homogeneous layer on a semi-infinite substrate. For the 200 and 600 grit roughness samples, the surface roughness thicknesses $d=\text{avg}_3(R_z)$, were measured to be 5 and 2.5 μm, respectively. The bulk thermal diffusivity of the untreated AISI-8620 steel was measured by photothermal radiometry in transmission[5] and the average value obtained for thermal diffusivity was 0.125 cm^2/s, which is within 0.005 cm^2/s of the documented value that exists for a similar low-carbon steel.[1]

The case depth of the samples is defined by 0.25% C on the carbon concentration profile, as shown in Fig. 2. The carbon profiles presented are given from a preprocess program written by B&W Heat Treating. It has been the experience of the company that the program predicts concentrations within $\pm 0.1\%$ carbon of the actual experimentally determined values. Carbon profoundly changes the phase-diagram relationships, microstructure, and properties in steels, and is the principal hardening element in all steel.[6] Carburizing is a high-temperature process by which the surface carbon concentration of a ferrous alloy is increased by diffusion. Slow cooling of plain carbon and low-alloy steels from the carburizing treatment results in a pearlitic microstructure in the case. This is a time-dependent nucleation and diffusion-controlled process where high-temperature austenite decomposes to form pearlite, a lamellar structure composed of ferrite and cementite. The strength of pearlite depends on the lamellar spacing where very slow-cooling rates produce a soft coarse pearlite while faster-cooling rates produce fine harder pearlite.

Rapid quenching in a liquid medium after carburizing results in a nonequilibrium martensite structure, the hardness of which is a function of its carbon content. Low-carbon martensites are soft while high-carbon martensites can be very hard. Figure 3 shows the microhardness profiles obtained for carburized and quenched AISI-8620 samples 34, 35, and 36, Table I. The carburized and slow-cooled samples exhibit low- and shallow-hardness profiles, whereas after quenching the profiles become higher and steeper. The depth of hardenability can be estimated from the quenched microhardness curves. Figure 3 shows that the case depth for the 0.02 in. (0.508 mm) case at around 550 HV quenched, is deeper than the predicted value. Since AISI-8620 is a low-alloy steel it has good hardenability, and thus the carburizing was probably done for a longer time, achieving a depth of up to 0.8 mm. This was an error that occurred at the plant. The other two case samples are within the predicted depths of 1.016 and 1.524 mm. The error bars for these microhardness tests lie between ± 10 HV for 300 HV and ± 20 HV for 700 HV. For the sake of clarity the last (deepest) measured value for the carburized samples in Fig. 3 is not shown. This value is 193 ± 7 HV at 3810 μm, which is the depth of saturation for the carburized samples.

These carburized and quenched samples have the same carbon diffusion profile as predicted in Fig. 2 since the carbon concentration is set as a function of depth in the carburizing process. Although both carburizing and quenching have the same carbon diffusion profile, the hardness profile in Fig. 3 is not the same. This is due to the fact that microhardness is a function of the mechanical properties of the sample, which are related to the microstructure of the material. This structure depends on the carbon diffusion profile and the quenching rates that are achieved in the heat-treatment process. The correlation that exists between the carbon concentration profile and the microhardness is a nonlinear empirical relationship with the main comparative similarity being a high-to-low-carbon concentration for a high-to-low microhardness (HV), respectively.

IV. EXPERIMENTAL RESULTS

Sequential experimental frequency scans in the range of 0.5 Hz–100 kHz were performed on the samples, which first underwent carburizing, and then quenching. For laser-beam modulation frequencies above 1000 Hz, strong surface-roughness effects were observed. The experimental surface-temperature response on the sample was normalized by the surface-temperature response of a reference sample (Zr alloy). This gave, for each frequency, an amplitude ratio and phase difference. The normalizing procedure was necessary to correct all instrumental frequency dependencies. Figure 4 shows all normalized experimental data for the carburized

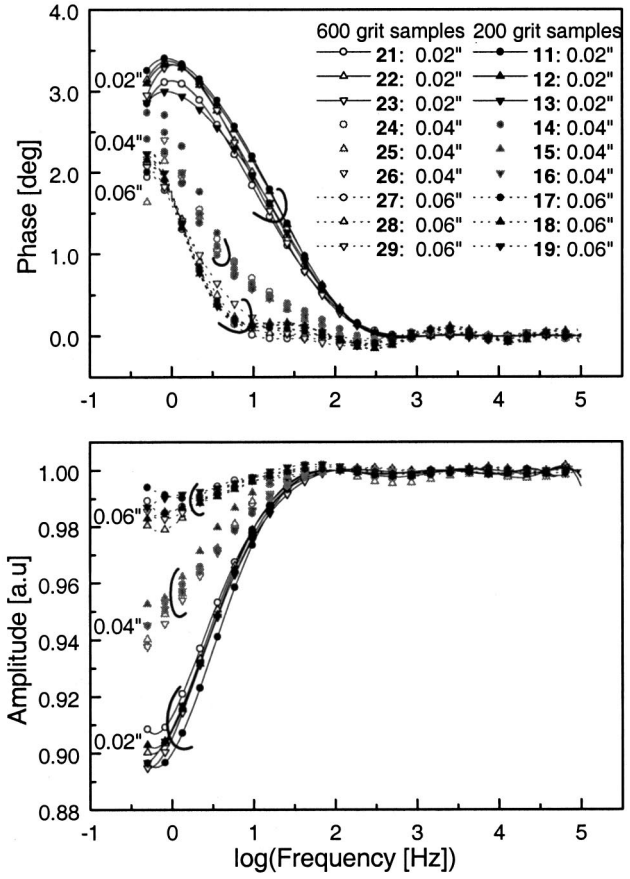

FIG. 4. Carburized AISI-8620 steel experimental data after numerical elimination of roughness for 0.02 in. (0.5 mm), 0.04 in. (1.0 mm), and 0.06 in. (1.5 mm) case depths with 2.5 μm (600 grit; open symbols) and 5 μm (200 grit; solid symbols) roughness.

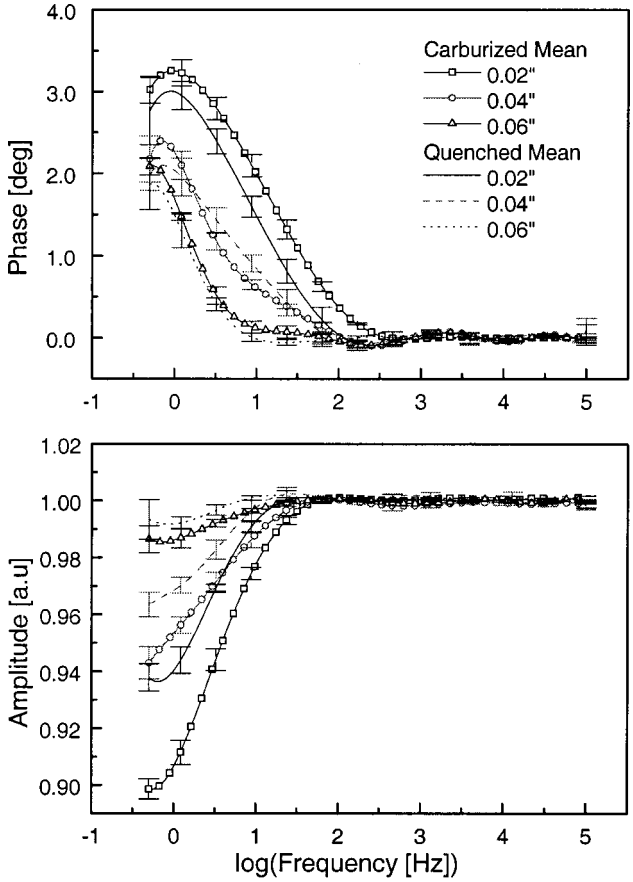

FIG. 5. Mean-frequency scans from carburized (open symbols) and quenched (lines) samples for 0.02 in. (0.5 mm), 0.04 in (1.0 mm), and 0.06 in. (1.5 mm) case depths.

samples with 200 and 600 grit roughness after a roughness elimination methodology[7] was applied. As a measure of the success of our roughness elimination method, Fig. 4 shows that the two different roughnesses resulted in the same inhomogeneous experimental responses for each of the three case depths, as expected.

After carburizing, the same samples were oil quenched and the frequency responses were obtained. Again, the same Gaussian roughness elimination[7] was applied on these data. The resulting average experimental curves over all three samples used in each carburizing and quenching process are shown Fig. 5. The sample-to-sample variances are indicated by the error bars. The experimental curves from the carburizing and quenching processes exhibit absolute signal (amplitude and phase) variations at low frequencies, yet, only small variations are observed in terms of the shapes of the curves. Furthermore, the back-propagation one-dimensional thermal-wave experiment only provides information about the *relative* thermal diffusivity of a material. The experimental data were reconstructed using the inverse-problem methodology developed in Ref. 8 as adapted to the present situation.[7] The bulk thermal diffusivities of both the carburized/slow-cooled and carburized/quenched samples were measured independently through radiometric backscattering experiments using a three-dimensional setup,[9] and were found to be different. The bulk thermal diffusivity of the *carburized/slow-cooled* samples was the same as the original untreated samples, $\alpha = 12.5 \times 10^{-6}$ m^2/s. The bulk thermal diffusivity of the *carburized/quenched* samples, however, was found to be $\alpha = 10.5 \times 10^{-6}$ m^2/s. This is due to the fact that the carburized/quenched samples have a low-carbon martensite structure in the bulk, whereas the carburized/slow-cooled samples have a ferritic/pearlitic structure. As a consequence, the absolute reconstructions shown in Fig. 6 for carburized/slow-cooled and carburized/quenched sample groups saturate at different diffusivity levels.

V. DISCUSSION

An important aspect of the reconstruction procedure is the understanding of the physical processes responsible for the apparent anticorrelation between thermal diffusivity and hardness in steels. This is a fundamental issue in light of earlier reports, in which both quantitative[3] and qualitative-only[2] agreements with microhardness-test-generated depth profiles in steels have been observed. Therefore, it was deemed important to determine which of the two major heat-treatment steps (carburization/slow cooling and carburization/quenching) in our steels was responsible, or dominant, for creating the reconstructed thermal-diffusivity depth profiles, and what were the relative contributions of both processes to those profiles. In general, the depth profiles

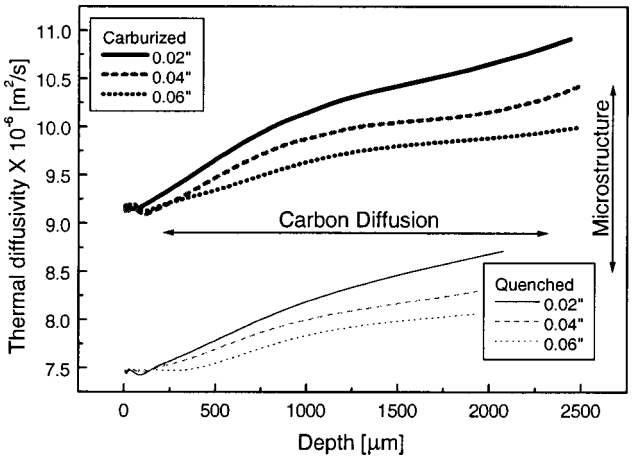

FIG. 6. Inverse-problem reconstructions of carburized (thick lines) and quenched (thin lines) from the mean-frequency scans of Fig. 5 for 0.02 in. (0.5 mm, solid), 0.04 in. (1.0 mm, dash), and 0.06 in. (1.5 mm, dot) case depth.

of the hardened samples exhibited anticorrelations between thermal diffusivity and hardness, which is consistent with the earlier findings in this and other laboratories.[2,3,10] In Fig. 7, the anticorrelation of hardness and thermal diffusivity is shown for (a) carburized and (b) quenched data. A good one-to-one anticorrelation between hardness and thermal diffusivity is present for the carburized/slow-cooled reconstructions [Fig. 7(a)], although the curves are not an exact mirror image of each other. This may be the result of the statistical variances of the frequency curves shown in Fig. 5: the mean curve in each case was used to reconstruct the thermal-wave depth profiles of Fig. 6. On the other hand, only one sample in each case was used to generate the microhardness depth profiles of Fig. 3. In Fig. 7(a), the reconstruction is shown down to a 1 mm depth, the region within which the carburized-steel hardness profile is available. Both the hardness and thermal-diffusivity profiles have not yet saturated to the bulk value. In the quenched data reconstructions [Fig. 7(b)], the quality of the one-to-one anticorrelation between microhardness and thermal diffusivity decreases with increasing depth. Beyond 2 mm, the hardness profiles approach the bulk value, but the diffusivity profiles do not yet saturate to the bulk thermal diffusivity. This could be due to the high sensitivity of photothermal methods in detecting actual small variations before reaching the bulk value (5 mm, for this case). The ever-increasing dispersion of the thermal-wave field with increasing depth undoubtedly contributes to some reconstruction uncertainty, typically, 5%–10% at depths greater than 1 mm.[8,11,12] Nevertheless, the exact mechanism of the thermal-diffusivity depth-profile generation can be investigated by comparing these reconstructions to the available hardness profiles. From Fig. 6, one can compare the thermal-diffusivity reconstructions between the carburized/slow-cooled and carburized/quenched data. It is seen that, although at different *absolute value* levels, the *depth distribution* of the thermal-diffusivity profiles for each case depth is similar. The quenched sample reconstructions are of lower absolute thermal-diffusivity value, because the quenched bulk thermal-diffusivity value is lower than that of the carburized bulk. For this reason, the thermal-diffusivity profiles for the quenched sample are somewhat shallower. This may be an artifact of the reconstruction algorithm,[8] in which each succeeding depth increment is determined by the local value of the previous thermal-diffusivity virtual slice. This tends to yield shallower depths for smaller thermal-diffusivity values. At the bulk value the same carbon content exists, but the carburized/slow-cooled samples have a ferritic/pearlitic structure, whereas the carburized/quenched samples have a martensitic structure. These structures result in different grain-boundary geometries,[6] and grain boundaries are known to affect both the local heat-transport rate as well as the resistance to mechanical penetration by the indenter. Therefore, a dependence of thermal diffusivity and hardness on microstructure is expected and observed in our experiments with AISI-8620. Typically, increased grain-boundary density due to microstructural changes decreases the transboundary heat flow with a concomitant decrease in thermal diffusivity. At the same time it increases the resistance of the grain-boundary network to mechanical penetration by an indenter, with a concomitant increase in hardness. These facts, along with the observed quantitative-diffusivity anticorrelation of the carburized-only samples with the hardness profile, Fig. 7(a), lead to the conclusion that in AISI-

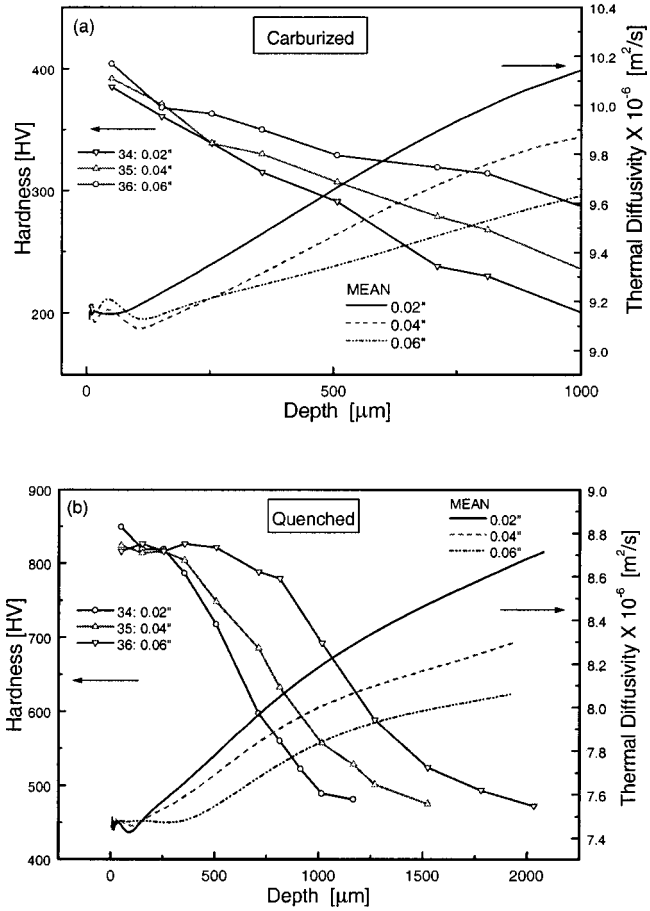

FIG. 7. (a) Hardness and thermal diffusivity profiles for carburized samples: 0.02 in. (0.5 mm, solid), 0.04 in. (1.0 mm, dash), and 0.06 in. (1.5 mm, dash-dot) case depths; (b) hardness and thermal-diffusivity profile for quenched samples: 0.02 in. (0.5 mm, solid), 0.04 in. (1.0 mm, dash), and 0.06 in. (1.5 mm, dash-dot) case depths.

8620 steel the microstructure dominates the *absolute values* of thermal diffusivity, whereas the (common) carbon diffusion profile (Fig. 2) controls the *depth distribution* of the thermal-diffusivity profiles in both carburized/slow-cooled and carburized/quenched steels. This is indicated pictorially in Fig. 6 where the microstructure determines the *absolute* thermal-diffusivity *value* along the *y* axis and the carbon diffusion along the depth (*x* axis) determines the *depth distribution*. Since the *depth distribution* is dominated by the carbon diffusion, it is then reasonable that the rate of saturation for the quenched samples is similar to that of carburizing samples, occurring at about 3.8 mm. The validity of these conclusions for other types of steel is not certain, and further studies of this type must be done in each case.

VI. CONCLUSIONS

In conclusion, thermal-wave depth profilometry can be an invaluable analytical technique for understanding the effect of surface-treatment processes such as case hardening of metals. In this work, AISI-8620 steel samples were subjected to common industrial heat treatments including carburizing and quenching. A complete experimental and theoretical/computational analysis was performed to generate thermal diffusivity depth profiles. This included a surface-roughness elimination technique,[7] which was proven effective for improving experimental data and achieving thermal diffusivity reconstructions of nonhomogeneous underlayers. The physical mechanism results of the present work can be insightful, in view of the apparent discrepancies found in the literature regarding the well-established, but physically little understood, anticorrelations between thermal-diffusivity (or conductivity) and hardness profiles, which sometimes are almost exact,[3] but often are not.[2,8,10] The present study of AISI-8620 steels concluded that the depth distribution of the thermal-diffusivity profile is dominated by carbon diffusion during carburization, whereas the absolute thermal-diffusivity value is dominated by microstructural changes incurred upon quenching the carburized steel. Obtaining the carbon diffusion profile nondestructively with thermal waves can be significant to the steel industry since, in the heat-treating process, the carbon content and diffusion profile are not measured outputs but only estimated inputs. These parameters can be easily extracted from the thermal-wave depth profiles through appropriate calibration of the curves shown in Fig. 7 against known hardness profiles.

ACKNOWLEDGMENT

The support of Materials and Manufacturing Ontario (MMO) is gratefully acknowledged.

[1] Y. S. Touloukian, R. W. Powell, C. Y. Ho, and M. C. Nicolaou, *Thermophysical Properties of Matter* (Plenum, New York, 1973), Vol. 10.
[2] M. Munidasa, F. Funak, and A. Mandelis, J. Appl. Phys. **83**, 3495 (1998).
[3] T. T. Lan, U. Seidel, and H. G. Walther, J. Appl. Phys. **77**, 4739 (1995).
[4] S. Paoloni, P. Mayr, C. Glorieux, R. Li Voti, H. Bentefour, and J. Thoen, Anal. Sci. (in press).
[5] L. Qian and P. Li, Appl. Opt. **29**, 4241 (1990).
[6] C. Hudson, *Structure and Metals* (Flarepath, U.K., 1973), Chap. 4.
[7] L. Nicolaides and A. Mandelis, J. Appl. Phys. (in press).
[8] A. Mandelis, F. Funak, and M. Munidasa, J. Appl. Phys. **80**, 5570 (1996).
[9] L. Nicolaides, M. Munidasa, and A. Mandelis, in *Topics On Nondestructive Evaluation Series*, edited by X. Maldague (ASNT, Columbus, Ohio, 1998), Vol. 3, pp. 65–69.
[10] Digest of the European Commission HARDPHOTOTEC Workshop on Hardness Measurements on Steel: Conventional and Alternative Nondestructive Methods, Ispra, Italy, 13–14 March 2000 (unpublished).
[11] J. Fivez and J. Thoen, J. Appl. Phys. **81**, 2963 (1997).
[12] C. Glorieux, R. Li Voti, J. Thoen, M. Bertolotti, and C. Sibilia, Inverse Probl. **15**, 1149 (1999).